2025 26th International Conference on Thermal, Mechanical and Multi-Physics Simulation and Experiments in Microelectronics and Microsystems (EuroSimE) | 979-8-3503-9300-2/25/$31.00 ©2025 IEEE | DOI: 10.1109/EUROSIME65125.2025.11006635

Finite Element Analysis and Experimental Investigation of Die-attach Fillet Influence on the Reliability of Epoxy-Based Pressure-Less Sintered Silver Joints

Xinyue Wang
Academy for Engineering & Technology
Fudan University
Shanghai, China
xywang22@m.fudan.edu.cn

Haixue Chen
Academy for Engineering & Technology
Fudan University
Shanghai, China
21210860001@m.fudan.edu.cn

Zhoudong Yang
Academy for Engineering & Technology
Fudan University
Shanghai, China
yangzd23@m.fudan.edu.cn

Jing Zhang
Heraeus Electronics
Heraeus Materials Technology Shanghai Ltd.
Shanghai, China
j.zhang@heraeus.com

Guoqi Zhang
Electronic Components, Technology, and Materials
Delft University of Technology
Delft, The Netherlands
g.q.zhang@tudelft.nl

Pan Liu*
Academy for Engineering & Technology
Fudan University
Shanghai, China
Corresponding: panliu@fudan.edu.cn

***Abstract*—This work investigated the impact of die-attach fillet geometry on the reliability of epoxy-based pressure-less sintered silver joints. Three types of sintered silver samples (Ag-0, Ag-1, and Ag-2) with 0%, 1%, and 2% epoxy content were prepared and characterized. Nanoindentation tests combined with inverse calculations were used to determine their elasto-plastic behavior. Fillet formation was influenced by organic solvent composition, dispense volume, and placement pressure, resulting in three geometries: rounded, triangular, and rounded rectangular. Finite element analysis was employed to simulate stress distribution and equivalent thermal strain under thermal cycling conditions (−55°C to 150°C). The simulation results were validated experimentally through shear strength testing and microstructural characterization using scanning electron microscopy (SEM). The findings highlight the significant role of fillet geometry, climbing height, and die-attach thickness in stress distribution and failure mechanisms, providing valuable insights into optimizing the die-attach process to enhance joint reliability in power electronics applications.**

Keywords—epoxy-based sintered silver, die-attach fillet, reliability, finite element analysis, thermal cycling test

I. INTRODUCTION

Die-attach plays a critical role in power electronics packaging, serving as a vital interconnect material in applications such as electric vehicles (EVs), renewable energy systems, and industrial motor drives. The reliability of power semiconductor modules relies on the mechanical integrity and thermal stability of the die-attach material, particularly under high temperatures and cyclic thermal stresses[1]. Among various die-attach materials, pressure-less sintered silver has gained interest due to its exceptional electrical conductivity, high melting point, and superior thermal stability. These characteristics make it a promising candidate for next-generation wide-bandgap (WBG) semiconductor devices, such as silicon carbide (SiC) power modules[2].

Despite its advantages, pressure-less sintered silver joints exhibit challenges during the die-attach process. One major issue is the migration of sintering material along the edges of the die, forming a die-attach fillet[3]. Factors such as surface tension, dispensing design, and placement pressure influence fillet formation. While a properly formed fillet enhances mechanical robustness, excessive fillet formation causes surface contamination, whereas insufficient paste dispensing leads to die lifting or cracking[4]. Additionally, epoxy content significantly affects mechanical properties, stress distribution, and interconnect performance[5]. Optimizing these factors is essential for ensuring the reliability and manufacturability of pressureless sintered silver joints.

In addition to fillet formation, other critical factors affecting the thermomechanical behavior include fillet shape, climbing height, and sintering layer thickness[3, 6]. Fillet shape influences stress distribution and crack initiation, with geometries such as rounded, triangular, and rounded rectangular fillets exhibiting different reliability levels[7]. Climbing height affects both mechanical support and stress dissipation—too low a height increases stress concentration and crack risk, while excessive height results in non-uniform adhesive distribution, weakening joint strength. Additionally, sintering layer thickness impacts thermal stress accumulation and interconnect reliability. Thin sintered layers are prone to stress concentration and early failure, while thick layers reduce heat dissipation efficiency, necessitating an optimized balance.

To address these challenges, this work investigates the effect of die-attach fillet geometry on the reliability of epoxy-based pressureless sintered silver joints using a combined finite element analysis (FEA) and experimental validation approach. Three types of sintered silver samples (0%, 1%, and 2% epoxy content) were prepared and characterized. Nanoindentation tests combined with inverse calculations were conducted to determine the elasto-plastic behavior and thermal strain under thermal cycling conditions. The impacts of different fillet shapes, climbing heights, and sintering layer thicknesses on joint reliability were analyzed through FEA, considering stress evolution during thermal shock cycles. Shear strength tests and scanning electron microscopy (SEM) analysis were performed to validate simulation results. The findings provide insights into optimizing the die-attach process by identifying the most suitable fillet shape, climbing height, and sintering layer thickness, contributing to improved reliability in power semiconductor packaging for extreme operating conditions.

II. Materials and Methodology

This section outlines the materials and methodology used to investigate the impact of die-attach fillet geometry on the reliability of epoxy-based pressureless sintered silver joints. The approach combines material characterization, FEA simulations, and experimental validation to assess the thermo-mechanical reliability under thermal cycling conditions.

A. Materials

The three types of sintered silver pastes, Ag-0, Ag-1, and Ag-2, were primarily composed of submicron silver particles and organic solvents, with epoxy resin contents of 0%, 1%, and 2% by weight, respectively. The metal component consisted of 500 nm silver particles at 85 wt%, ensuring uniform dispersion and stability. The solvent system included polyethylene glycol and pinene alcohol, which facilitated proper rheology and dispersion. The epoxy system comprised bisphenol A epoxy resin, with methyltetrahydrophthalic anhydride (WNY-1021) as the curing agent and 2-ethyl-4-methylimidazole (EMI-2,4) as an accelerator to enhance cross-linking and polymerization efficiency.

To ensure uniform dispersion, initial mixing was performed using a mortar, followed by planetary mixing (THINKY ARE-310) to eliminate agglomerates and optimize paste consistency.

Epoxy-based pressureless sintered silver joints were fabricated using a benchtop dispenser (Musashi NX320), an automatic pick-and-place machine (BESI Datacon 2200 evo), and a Binder M115 oven for sintering. The samples were sintered at 260°C for 120 minutes in a nitrogen atmosphere. The joints were formed on an active metal brazing (AMB) substrate using a 4×4 mm² silver-plated silicon dummy chip with a 320 µm thickness.

B. Fillet Formation

The effects of different die-attach processes on fillet formation were investigated by varying placement pressure and dispense volume. For each combination of sintering paste and processing condition, ten joints were prepared for subsequent analysis. Three dispensing gas pressures (120 kPa, 140 kPa, and 160 kPa) and three bonding pressures (80 g, 100 g, and 120 g) were tested. The sintered joint samples were sectioned, polished, and subjected to cross-sectional analysis.

Fillets were classified into three distinct geometries: rounded, triangular, and rounded rectangular, as shown in Fig. 1. The sintered layer thickness of most samples was between 30 µm and 70 µm, while the fillet height was primarily distributed between 100 µm and 175 µm.

C. Methodology

1) Nanoindentation and Inverse Calculation

To derive the constitutive equations of the three types of sintered silver materials, nanoindentation tests combined with inverse calculations were conducted. This approach enables precise characterization of the elastic-plastic behavior of materials under varying loading conditions. The tests were performed on sintered silver samples with 0%, 1%, and 2% epoxy content, fabricated using the specified sintering pastes.

During the tests, a sharp indenter applied controlled forces to the surface of the sintered silver samples, while indentation depth and force data were continuously recorded to evaluate

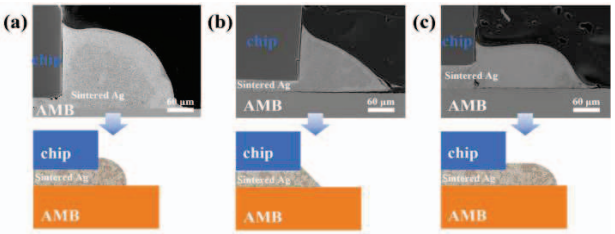

Fig. 1. Schematic diagram of adhesive fillet shapes: (a) Rounded corner fillet; (b) Triangular fillet; (c) Rounded rectangular fillet.

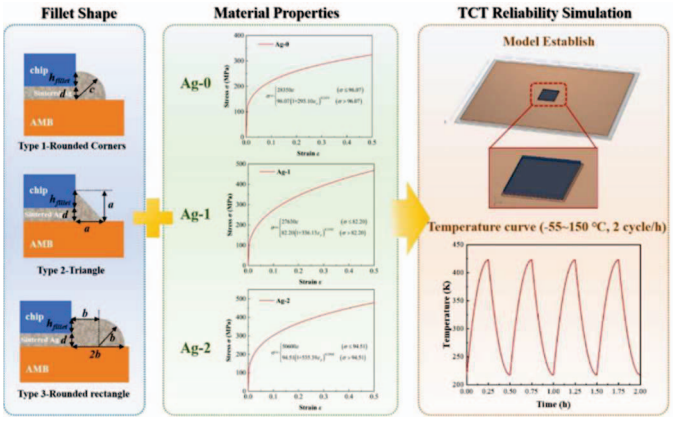

Fig. 2. Schematic diagram of finite element model establishment.

hardness and elastic modulus. The collected data were then processed using inverse calculations to derive the stress-strain constitutive equations, essential for understanding the elasto-plastic response of sintered silver under operational conditions.

The inverse calculation process involved fitting the experimental nanoindentation data to a numerical model of the material's mechanical behavior, following the approach detailed in previous studies[8, 9]. The resulting constitutive equations for Ag-0, Ag-1, and Ag-2 are as follows:

Ag-0:

$$\sigma = \begin{cases} 28350\varepsilon & \sigma \le 96.07\ \text{MPa} \\ 96.07\left(1 + 295.1\varepsilon_p\right)^{0.2431} & \sigma > 96.07\ \text{MPa} \end{cases} \quad (1)$$

Ag-1:

$$\sigma = \begin{cases} 27630\varepsilon & \sigma \le 82.20\ \text{MPa} \\ 82.20\left(1 + 336.13\varepsilon_p\right)^{0.3392} & \sigma > 82.20\ \text{MPa} \end{cases} \quad (2)$$

Ag-2:

$$\sigma = \begin{cases} 50600\varepsilon & \sigma \le 94.51\ \text{MPa} \\ 94.51\left(1 + 535.39\varepsilon_p\right)^{0.2904} & \sigma > 94.51\ \text{MPa} \end{cases} \quad (3)$$

These constitutive equations provide critical insights into the mechanical properties of sintered silver and serve as key inputs for subsequent finite element simulations, facilitating the analysis of stress distribution and thermal strain in the joints.

2) Finite Element Analysis

The finite element model was developed using COMSOL Multiphysics 5.6 to simulate the thermo-mechanical behavior of pressureless sintered silver joints under thermal cycling conditions. This study primarily focuses on analyzing the

thermal stress-strain response of the sintered silver layer and its distribution within the die-attach joints. The solid mechanics and heat transfer modules in COMSOL were employed to simulate the thermal and mechanical interactions within the joint structure. Fig. 2 presents an overview of the methodology.

The joint geometry was simplified into a three-layer sandwich structure consisting of a silicon chip, sintered silver layer, and an active metal brazing (AMB) substrate, as shown in Fig. 3. This simplification ensures a realistic approximation of actual performance while maintaining computational feasibility.

For accurate simulation, sintered silver layer dimensions were carefully defined. As shown in Fig. 2, key parameters include sintered layer thickness (d) and fillet height (h_{fillet}). The fillet shape was categorized into three distinct geometries: rounded, triangular, and rounded rectangle. The rounded fillet was approximated as a quarter circle with a radius of c, the triangular fillet was modeled as an isosceles triangle with side length a, and the rounded rectangle fillet was approximated as a rectangle with a 2:1 aspect ratio and a corner radius of b. The dimensions of a, b, and c were determined as:

$$a, b, c = d + h_{fillet} \tag{4}$$

These parameters were used to analyze the influence of fillet geometry on stress distribution in the joint during thermal cycling. The experimental design parameters are detailed in Table 2.

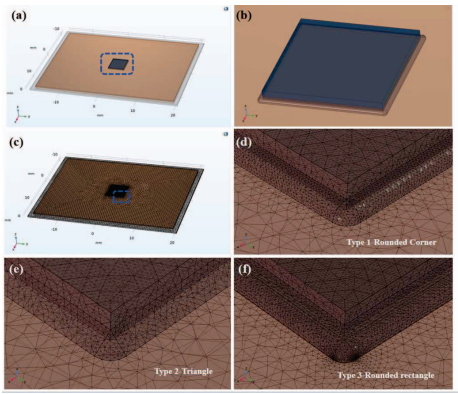

Fig. 3. (a, c) Overall view of the 3D mocdel and mesh division; (b, d, e, f) Local schematic diagram and mesh division.

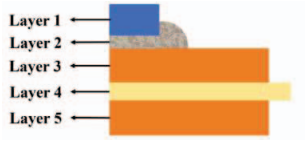

Fig. 4. Cross-sectional view of the quarter finite element model of the pressure-less sintered silver joint.

TABLE I. MATERIAL PROPERTIES OF THE FINITE ELEMENT SIMULATION MODEL

Material	Dimension (mm^3)	K ($W/m^{-1}/K^{-1}$)	CTE (ppm/°C)	E (GPa)
Si	4*4*0.32	150	2.6	180
Sintered Silver	Table 2	86~91	3.17~16.7	87~93
Cu	24.8*35.8*0.3	400	17	122
Al_2O_3	27*38*0.32	47	8.1	340

Following the geometric setup, material properties and initial conditions were assigned to the model. Fig. 4 presents a cross-sectional view of a quarter of the model. The materials used in the simulation include silicon, sintered silver, copper,and aluminum oxide (Al_2O_3), with their corresponding properties listed in Table 1. The model assumes isotropic and homogeneous material properties, neglecting microstructural variations such as porosity and grain size effects.

Subsequently, the model was meshed to improve accuracy and precision in simulation, as shown in Fig. 3. Proper mesh refinement is essential for optimizing the design and providing detailed insights into stress and strain distributions.

In the FEA simulations of pressureless sintered silver joints under thermal cycling conditions, appropriate boundary conditions were applied to ensure realistic thermomechanical behavior. The model was subjected to temperature cycling between -55°C and 150°C following the JEDEC JESD22-A104E standard, with a uniform temperature load applied across all components to simulate thermal expansion and contraction. The model was subjected to 250 hours of thermal cycling at a rate of 2 cycles per hour, totaling 500 cycles. To balance computational accuracy and efficiency, the solver time step was set to 25 hours. Mechanically, the bottom of the substrate was fixed in all directions (Ux = Uy = Uz = 0) to prevent rigid body motion, and the chip-silver interface was assumed to be fully bonded, ensuring stress transfer during thermal cycling. A free expansion condition was applied to all materials, allowing for thermomechanical strain based on their respective coefficients of thermal expansion (CTE). The interface between the sintered silver layer and the chip/substrate was modeled with perfect bonding, while a frictionless contact condition was imposed at the fillet region to enable stress redistribution. These boundary conditions provide a realistic representation of stress evolution in the die-attach joint under thermal cycling.

Upon completing the simulation, various output parameters were extracted for analysis, including maximum thermal stress, equivalent thermal strain, and stress distribution contours. These results provide crucial insights into failure mechanisms, particularly in relation to stress concentration and crack propagation under thermal shock conditions, which directly affect the reliability of power semiconductor interconnects.

3) Experimental Tests

The high-frequency switching characteristics of high-power semiconductor devices subject power modules to prolonged cyclic thermal loads in practical applications. Evaluating the thermomechanical reliability of pressureless sintered silver joints, which serve as chip interconnect materials, is therefore essential. In this study, thermal cycling tests (TCT) were conducted using a VT37006S2 temperature cycling chamber to assess joint durability under thermal shock conditions. The tests followed JEDEC JESD22-A104E standards, with temperature cycling between -55°C and 150°C at a rate of 2 cycles per hour for a total of 500 cycles, ensuring consistency with FEA conditions.

To evaluate the mechanical integrity of the joints, push-pull shear strength tests were conducted using a Dage 4000Plus multifunctional solder strength tester (Nordson, UK). The initial shear strength values were 5.75 MPa for Ag-0, 15.07 MPa for Ag-1, and 18.46 MPa for Ag-2. After 500

TABLE II. GEOMETRIC PARAMETER SETTINGS FOR MODEL DESIGN

Experiment No.	Sintered Silver Type	Fillet Type	Mmorphology Parameters of Fillet (μm)			Thickness of Sintering Layer *d* (μm)	Fillet Height h_{fillet} (μm)
			a	*b*	*c*		
Group 1	Ag-0	1	-	-	175	50	125
Group 2	Ag-0	2	175	-	-	50	125
Group 3	Ag-0	3	-	175	-	50	125
Group 4	Ag-1	1	-	-	175	50	125
Group 5	Ag-1	2	175	-	-	50	125
Group 6	Ag-1	3	-	175	-	50	125
Group 7	Ag-2	1	-	-	175	50	125
Group 8	Ag-2	2	175	-	-	50	125
Group 9	Ag-2	3	-	175	-	50	125
Group 10	Ag-2	1	-	-	125	50	75
Group 11	Ag-2	1	-	-	150	50	100
Group 12	Ag-2	1	-	-	200	50	150
Group 13	Ag-2	1	-	-	225	50	175
Group 14	Ag-2	1	-	-	180	30	150
Group 15	Ag-2	1	-	-	190	40	150
Group 16	Ag-2	1	-	-	210	60	150
Group 17	Ag-2	1	-	-	220	70	150

thermal shock cycles, the shear strength decreased to 4.70 MPa for Ag-0, 13.78 MPa for Ag-1, and 16.60 MPa for Ag-2. The results confirm that the Ag-2 joints (2 wt% epoxy content) exhibited superior thermal cycling resistance, maintaining the highest mechanical stability throughout the thermal cycling process. This enhanced performance is attributed to the optimized epoxy content, which improves interfacial adhesion by effectively filling particle gaps without obstructing neck formation, thereby reinforcing joint integrity and mitigating stress-induced degradation.

To further examine joint performance, remaining samples were sliced and polished for cross-sectional analysis, assessing interface bonding using an MM-400 metallographic microscope (Nikon, Japan) and a Gemini 300 field emission SEM (Zeiss, Germany), providing detailed microstructural characterization of sintered silver joints.

III. Results and Discussion

To comprehensively analyze the influence of adhesive conditions on stress distribution during thermal cycling and its impact on joint shear strength, this section presents a combined finite element simulation and experimental validation approach. The findings highlight the critical role of precise process control in enhancing the thermomechanical reliability of power electronic interconnects.

A. Effects of Fillet Shape on Sintered Silver Joints

The influence of three adhesive fillet geometries on the thermal stress distribution of pressureless sintered silver joints was systematically examined. Fig. 5 presented the simulated thermal stress distribution after 500 thermal shock cycles within a temperature range of -55°C to 150°C. The results indicated a significant increase in thermal stress following thermal cycling, primarily due to the accumulation of plastic deformation in the sintered silver layer. Comparative analysis revealed that joints with a rounded rectangular fillet exhibited the highest thermal stress concentration, followed by triangular and rounded fillet geometries. Notably, the rounded fillet achieved the most uniform thermal stress distribution, minimizing localized stress accumulation.

The equivalent thermal strain values obtained from the finite element simulation were compared with experimental reliability data for the Ag-2 joints under different fillet shapes,

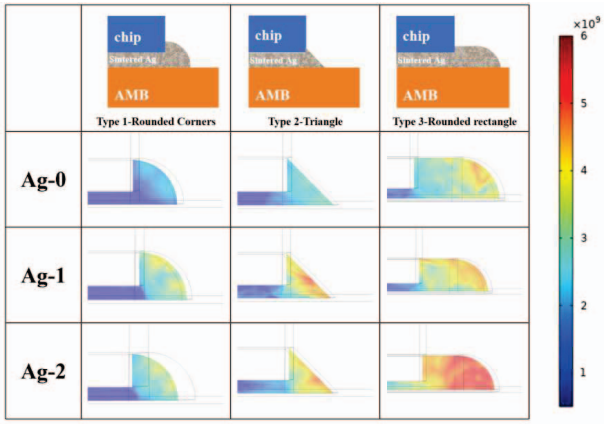

Fig. 5. Thermal stress distribution contours of sintered silver joints cross-sections with different adhesive fillet shapes.

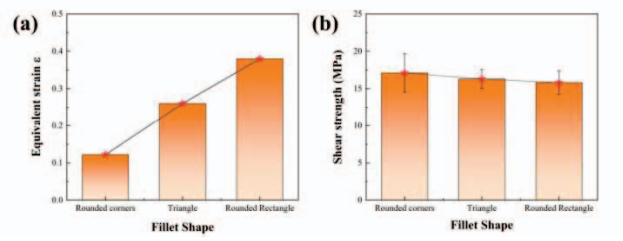

Fig. 6. Pressure-less sintered silver joints with different adhesive fillet shapes: (a) Equivalent strain; (b) Shear strength.

as shown in Fig. 6. Fig. 6(a) illustrated that joints with a rounded fillet shape exhibited the lowest equivalent thermal strain, followed by triangular and rounded rectangular fillets. Lower thermal stress and strain suggested a reduced risk of crack initiation and propagation under long-term cyclic thermal loads, indicating superior mechanical properties such as shear strength. These findings confirmed that the rounded fillet provided superior thermomechanical reliability in extended thermal shock conditions

Further validation was conducted through shear strength testing on epoxy-based pressureless sintered silver Ag-2 joints with different fillet shapes after 500 thermal shock cycles (Fig. 8(b)). Among the three configurations, rounded fillets exhibited the highest shear strength, followed by triangular and rounded rectangular fillets, with average values of 17.1 MPa, 16.3 MPa, and 15.81 MPa, respectively. The experimental measurement results are consistent with the simulation results, verifying the accuracy of the model.

B. Effect of Paste Climbing Height on Sintered Silver Joints

Building upon the preceding analysis of fillet geometry, this section presents a thermomechanical evaluation of epoxy-based pressureless sintered silver Ag-2 joints with rounded climbing shapes. In the finite element (FE) thermomechanical model, the sintered layer thickness was maintained at 50 µm, while the adhesive climbing height was varied at 75 µm, 100 µm, 125 µm, 150 µm, and 175 µm. Fig. 7 illustrated the simulated thermal stress distribution across the cross-section of the Ag-2 joints after thermal shock testing. The results indicated that as the climbing height increases, the thermal stress distribution initially becomes more uniform but eventually re-concentrated. The highest stress concentration occurred at 75 µm, whereas at 150 µm, the stress distribution was relatively uniform, minimizing localized stress accumulation.

To validate the simulation results, equivalent thermal strain values obtained from FEA were compared with experimentally measured reliability data for Ag-2 joints, as shown in Fig. 8. Fig. 8(a) presented the simulated equivalent thermal strain values across different climbing heights. Between 75 µm and 175 µm, the strain first decreased, reached a minimum at 150 µm, and then increased again. This trend was attributed to the combined effects of improved thermal stress distribution and material densification limitations. Increasing the climbing height facilitated a more even distribution of thermal stress, reducing strain and providing additional mechanical support to the chip, thereby enhancing interconnect strength. However, an excessively high climbing height leaded to increased outflow of sintered silver, which affected the decomposition and volatilization of organic components within the sintered layer, hindering densification at the microstructural level and negatively impacting interconnect strength. These effects established an optimal balance at 150 µm, where equivalent thermal strain reached its lowest point. A lower equivalent thermal strain corresponded to a reduced risk of crack initiation and propagation under cyclic thermal loading, indicating enhanced long-term reliability and mechanical stability in thermal shock environments.

To further validate FEA predictions, shear strength tests were conducted on Ag-2 joints after 500 thermal shock cycles (Fig. 8(b)). As climbing height increased from 115 µm to 145 µm, shear strength improved from 12.3 MPa to 15.1 MPa. The correlation between FE simulations and experimental measurements further confirms the FE model's accuracy.

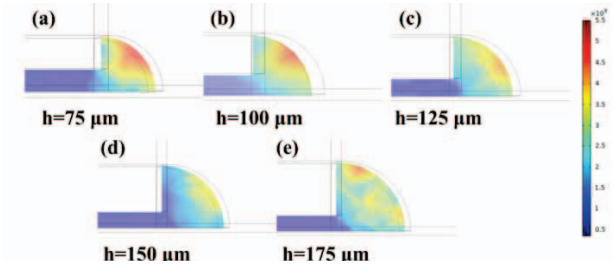

Fig. 7. Thermal stress distribution contours of sintered silver joints cross-sections at different adhesive climbing heights.

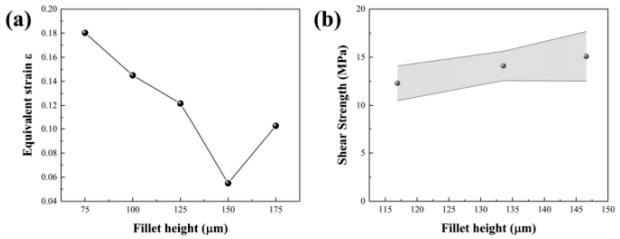

Fig. 8. Pressureless Ag-2 sintered silver joint samples at different climbing heights: (a) Simulated equivalent thermal strain; (b) Measured shear strength.

C. Effect of Sintering Layer Thickness on Sintered Silver Joints

The thermomechanical properties and crack behavior of sintered silver joints are significantly influenced by the sintered layer thickness, as it governs the propagation of both interface and vertical cracks. This section provides a comprehensive evaluation of the long-term reliability of sintered silver layers in bonded power chips by analyzing thermal stress distribution and its evolution during thermal shock cycling for various sintered layer thicknesses.

In the FE model, an optimized rounded fillet shape with a 150 µm fillet height was selected based on findings from previous sections, while the sintered layer thickness was varied at 30 µm, 40 µm, 50 µm, 60 µm, and 70 µm. Fig. 9 illustrated the simulated thermal stress distribution at the upper and lower interfaces and fillet regions of epoxy-based pressureless sintered silver Ag-2 joints after 500 thermal shock cycles. The results indicated that maximum thermal stress was primarily concentrated at the corners and edges of the sintered layer, particularly in the fillet region, while the central region experienced relatively lower stress. As the sintered layer thickness increased from 30 µm to 70 µm, both the peak thermal stress and stress distribution became more uniform within the sintered silver layer, reducing localized stress accumulation.

Equivalent thermal strain values from FEA were compared with experimentally measured shear strength data for Ag-2 joints (Fig. 10). Fig. 10(a) presented the simulated equivalent thermal strain values for Ag-2 joints after 500 thermal shock cycles. The results demonstrated that as the sintered layer thickness increases from 30 µm to 70 µm, the equivalent thermal strain decreased, indicating enhanced interconnection strength and reliability. Conversely, reducing the sintered layer thickness led to increased strain. Once a

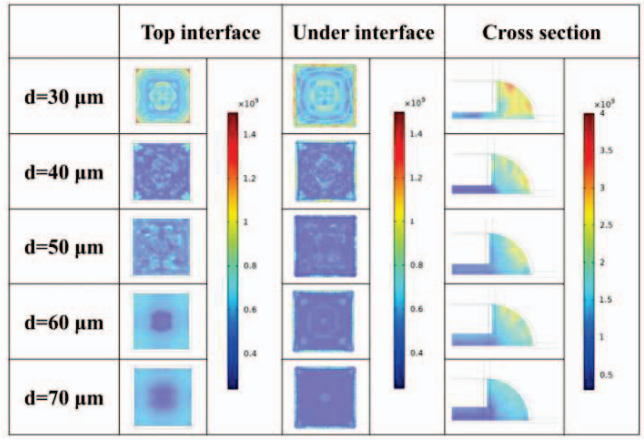

Fig. 9. Thermal stress distribution contours of sintered silver layers at the upper and lower interfaces for different sintered layer thicknesses.

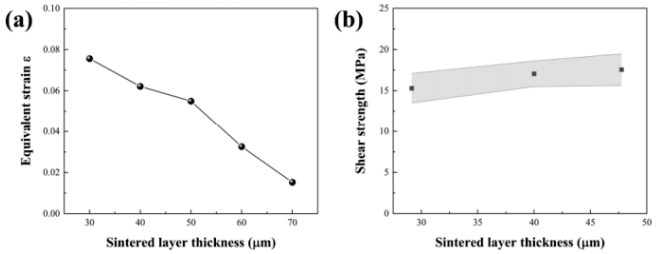

Fig. 10. Pressureless Ag-2 sintered silver joints with different sintered layer thicknesses: (a) Equivalent thermal strain; (b) Shear strength.

critical strain threshold was exceeded, the probability of crack initiation and propagation increased, eventually leading to shear strength degradation. Excessive strain accumulation resulted in a complete loss of shear strength, confirming that strain accumulation is a primary factor driving the mechanical deterioration of sintered silver joints.

To validate the FEA results, shear strength tests were performed on epoxy-based pressureless sintered silver Ag-2 joints with varying sintered layer thicknesses under identical conditions: 4×4 mm² chip interconnect area, 320 μm chip height, and 150 μm rounded fillet shape. Fig. 10(b) presented the shear strength results, which indicated that as the sintered layer thickness increased from 30 μm to 50 μm, the shear strength increased from 15.3 MPa to 17.6 MPa. Joints with thinner sintered layers exhibited slight delamination and crack propagation, likely attributed to accumulated plastic strain. The strong agreement between simulated and experimental results further supports the accuracy of the model.

D. Limitations and Future Optimization

While the finite element model effectively predicts thermal stress distribution and mechanical properties, certain assumptions limit accuracy. The model assumes uniform material properties, neglecting variations in porosity and grain size, which influence mechanical behavior. Additionally, real-world operating conditions such as dynamic temperature fluctuations and external mechanical loads were not considered. Future work should integrate multiphysics simulations, incorporating mechanical, thermal, and electrical interactions to achieve more realistic performance predictions for power electronic interconnects.

IV. Conclusions

This study investigated the impact of epoxy content, die-attach processes, and key design parameters on the reliability of epoxy-based pressureless sintered silver joints, integrating FEA simulations and experimental validation. The Ag-2 sample (2 wt% epoxy) exhibited the highest mechanical performance, with an initial shear strength of 18.46 MPa. After thermal cycling, shear strengths decreased to 4.7 MPa (Ag-0), 13.78 MPa (Ag-1), and 16.6 MPa (Ag-2), confirming Ag-2's superior thermal cycling resistance.

Fillet geometry played a critical role in stress distribution and failure mechanisms. FEA simulations demonstrated that rounded fillets resulted in the most uniform thermal stress distribution, minimizing localized stress accumulation and reducing the risk of crack initiation. Experimental shear strength tests validated these predictions, confirming rounded fillets as the optimal configuration. Additionally, climbing height and sintered layer thickness significantly affected mechanical stability. A 150 μm climbing height achieved balanced stress distribution, while increasing sintered layer thickness to 70 μm reduced thermal strain, enhancing joint reliability. The strong correlation between FEA predictions and experimental results confirmed the accuracy of the thermomechanical model.

In summary, this work focuses on the critical role of fillet geometry in determining joint reliability, providing insights into the interplay between epoxy content, fillet formation, and sintering process parameters. The formation of different fillet shapes in samples is influenced by factors such as surface tension, viscosity, and wetting properties, which require further investigation. Future research should explore the relationship between epoxy formulation and fillet evolution to refine process control and enhance interconnect reliability in high-performance power electronics.

Acknowledgment

In this work, the authors would like to thank National Natural Science Foundation of China (Grant 62304051), Shanghai Science & Technology Commission (Grant 24500790700), Doctoral Student Program of the Young Elite Scientists Sponsorship Program by CAST (2024), and Shanghai SiC Power Devices Engineering & Technology Research Center (19DZ2253400) for funding this research. Many thanks to Chat Generative Pre-Trained Transformer (ChatGPT, OpanAI) for language help.

References

[1] S. L. Zhao, Y. Tong, C. B. Wang, and E. R. Yao, "Challenges and progress in packaging materials for power modules with high operation temperature: Review," (in English), *Journal of Materials Science-Materials in Electronics,* Review vol. 35, no. 35, p. 30, Dec 2024, Art. no. 2237.

[2] Z. Cui *et al.*, "Review on Shear Strength and Reliability of Nanoparticle Sintered Joints for Power Electronics Packaging," (in English), *Journal of Electronic Materials,* Review vol. 53, no. 6, pp. 2703-2726, Jun 2024.

[3] L. Bu, W. L. Ching, H. S. Ling, M. W. Rhee, and Y. P. Fen, "3-D Modeling and Characterization for Die Attach Process," *Ieee Transactions on Components Packaging and Manufacturing Technology,* Article vol. 6, no. 10, pp. 1567-1575, Oct 2016.

[4] J. Weidler, R. Newman, C. J. Zhai, and I. Ieee; Ieee, "Optimizing assembly factors to minimize interlayer die stress in a PBGA package," in *52nd Electronic Components and Technology Conference (ECTC)*, San Diego, Ca, pp. 1172-1177, 2002.

[5] X. Wang, Z. Zeng, G. Zhang, J. Zhang, and P. Liu, "Joint Analysis and Reliability Test of Epoxy-Based Nano Silver Paste Under Different

Pressure-Less Sintering Processes," *Journal of Electronic Packaging,* vol. 144, no. 4, 2022.

[6] C. Lo, O. K. Yoke, C. C. Yong, L. B. Seong, and Ieee, "Assembly Challenges for Low Modulus Die Attach Material for MEMS Devices," in *11th Electronics Packaging Technology Conference*, Shangri La, SINGAPORE, 2009, pp. 762-767, 2009.

[7] L. Ji, L. C. Wai, M. W. D. Rhee, and Ieee, "Flow modeling of die attach process and the optimization of process parameters in advance packaging," in *14th IEEE Electronics Packaging Technology Conference (EPTC)*, Singapore, SINGAPORE, 2012, pp. 379-383, 2012.

[8] H. Chen, X. Wang, Z. Zeng, G. Zhang, J. Zhang, and P. Liu, "Solvent modulation, microstructure evaluation, process optimization, and nanoindentation analysis of micro-Cu@Ag core–shell sintering paste for power electronics packaging," *Journal of Materials Science: Materials in Electronics,* vol. 34, no. 24, 2023.

[9] X. Wang *et al.*, "Microstructure evolution and micromechanical behavior of solvent-modified Cu–Ag composite sintered joints for power electronics packaging at high temperatures," *Journal of Materials Research and Technology,* vol. 30, pp. 8433-8450, 2024.